Claremont Colleges
Scholarship @ Claremont

HMC Senior Theses | HMC Student Scholarship

2003

Ridge Coarsening in Evaporatively Driven Climbing Films

Peter Lamb
Harvey Mudd College

Recommended Citation
Lamb, Peter, "Ridge Coarsening in Evaporatively Driven Climbing Films" (2003). *HMC Senior Theses*. 150.
https://scholarship.claremont.edu/hmc_theses/150

This Open Access Senior Thesis is brought to you for free and open access by the HMC Student Scholarship at Scholarship @ Claremont. It has been accepted for inclusion in HMC Senior Theses by an authorized administrator of Scholarship @ Claremont. For more information, please contact scholarship@cuc.claremont.edu.

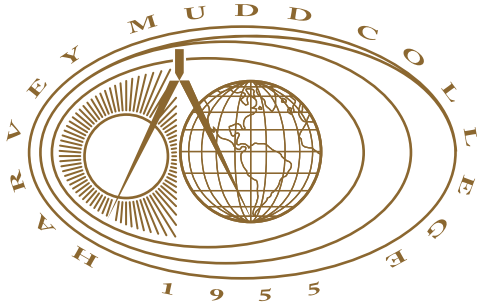

Ridge Development and Coarsening in Evaporatively-Driven Climbing Films

by

Peter J. Lamb
Ali Nadim, Advisor

Advisor: _____

Second Reader: _____

(Andrew Bernoff)

May 2003

Department of Mathematics

HARVEY MUDD COLLEGE

Abstract

Ridge Development and Coarsening in Evaporatively-Driven Climbing Films

by Peter J. Lamb

May 2003

In thin-film mixtures of alcohol and water, differences in evaporation rates and surface tensions between the two liquids can cause what is known as Marangoni convection within the fluid. This can lead to the formation of interesting instabilities on the surface of the film, such as the commonly observed "wine tears" phenomenon.

Similar instabilities are observed when an inclined plate is immersed in a water-alcohol reservoir. In addition to the tears, small ridges can be observed where the thin-film along the side of the plate rejoins the larger reservoir. These ridges slowly drift to the side and merge with other ridges, coarsening into larger ones.

Using lubrication theory, Hosoi and Bush developed a one-dimensional model of the ridge instability which takes into account gravity, capillarity and Marangoni stresses at the surface of the film and results in a fourth-order non-linear partial differential equation describing the height of the ridges as a function of time and position along the plate. Two different but complementary numerical models were implemented to solve their equation. Both models are able to show development of ridges from random initial conditions as well as lateral ridge movement and coarsening. In addition to the numerical approaches some analysis was done on the equation to gain further insight into the nature of the ridge coarsening.

Table of Contents

List of Figures

List of Tables

Acknowledgments

I would like to especially thank Professor Ali Nadim for advising me this year as well as Professor Anette Hosoi for getting me started on this continuation of her research the summer of 2002. I would also like to thank Professor Andrew Bernoff for agreeing to be my second reader and for his helpful comments both last summer and this year.

I would also like to thank my parents and the rest of my family for their unwavering love and support.

Chapter 1

Introduction

When wine is swirled up the side of a glass, the fluid convects up the sides where it beads up on the leading edge, eventually dripping down. This phenomenon of wine "tears" or "legs" has fascinated people for a long time.

The same effect and additional surface instabilities can be observed when an inclined plate is immersed in a reservoir containing an alcohol-water mixture as shown in Figure 1.1. In addition to the tears which form, other interesting instabilities form on the surface of the thin film on the side of the plate. At the base of the film, where the plate emerges from the liquid reservoir, small ridges form, eventually drifting sideways and merging with each other into coarser ridges. These instabilities can be seen in the pictures taken by Hosoi and Bush and shown in Figure 1.2.

The mechanism driving these surface instabilities is what is known as Marangoni convection. Differences in surface tension and evaporation rates between water and alcohol lead to surface tension gradients along the free boundary of the film. Alcohol evaporates more quickly, and has a lower surface tension than water. Parts of the film further up the side of the plate have had the alcohol evaporating for longer, resulting in a higher concentration of water and higher surface tension further up the side. This tends to draw more of the fluid up the plate, eventually beading up at the leading edge and forming tears. When the film is perturbed upward from its steady-state, it has a higher water-concentration and higher surface

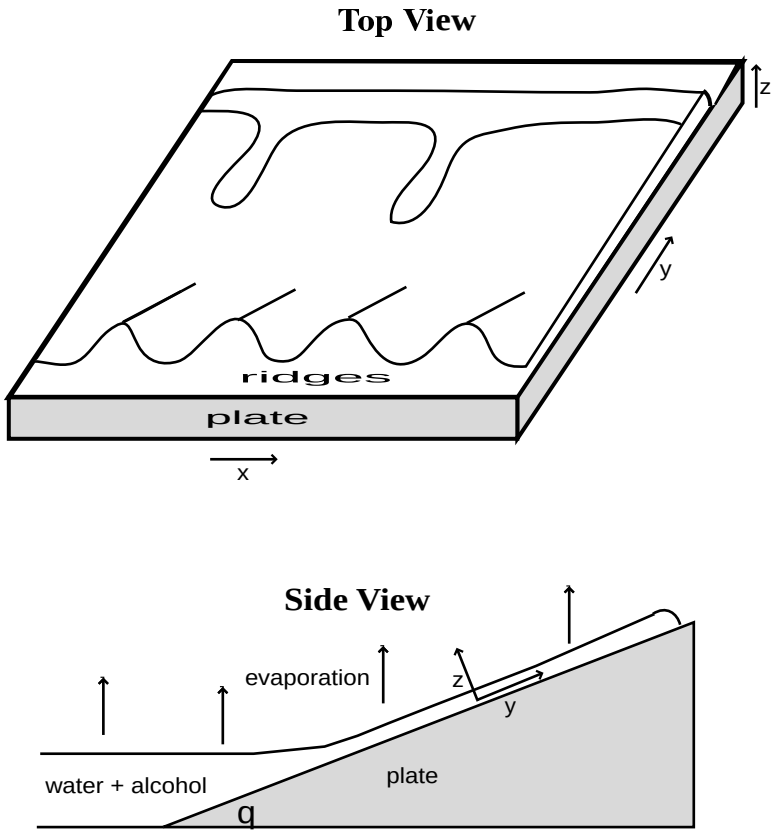

Figure 1.1: Physical setup

tension at that point, drawing up fluid and forming ridges. Studying the formation and evolution of these ridges is the focus of this thesis.

Historical background and approaches to this system are described in the paper by Hosoi and Bush [8]. They develop a one-dimensional model describing the formation and evolution of the ridges, and it is upon this model that the majority of this work is based. Chapter 2 presents their model and another more generalized approach I undertook towards deriving a governing equation for the system. Chapter 3 of this paper describes the analytical approaches taken to gain further insight into these equations, and Chapter 4 presents the numerical models developed to solve these equations and the results from those models.

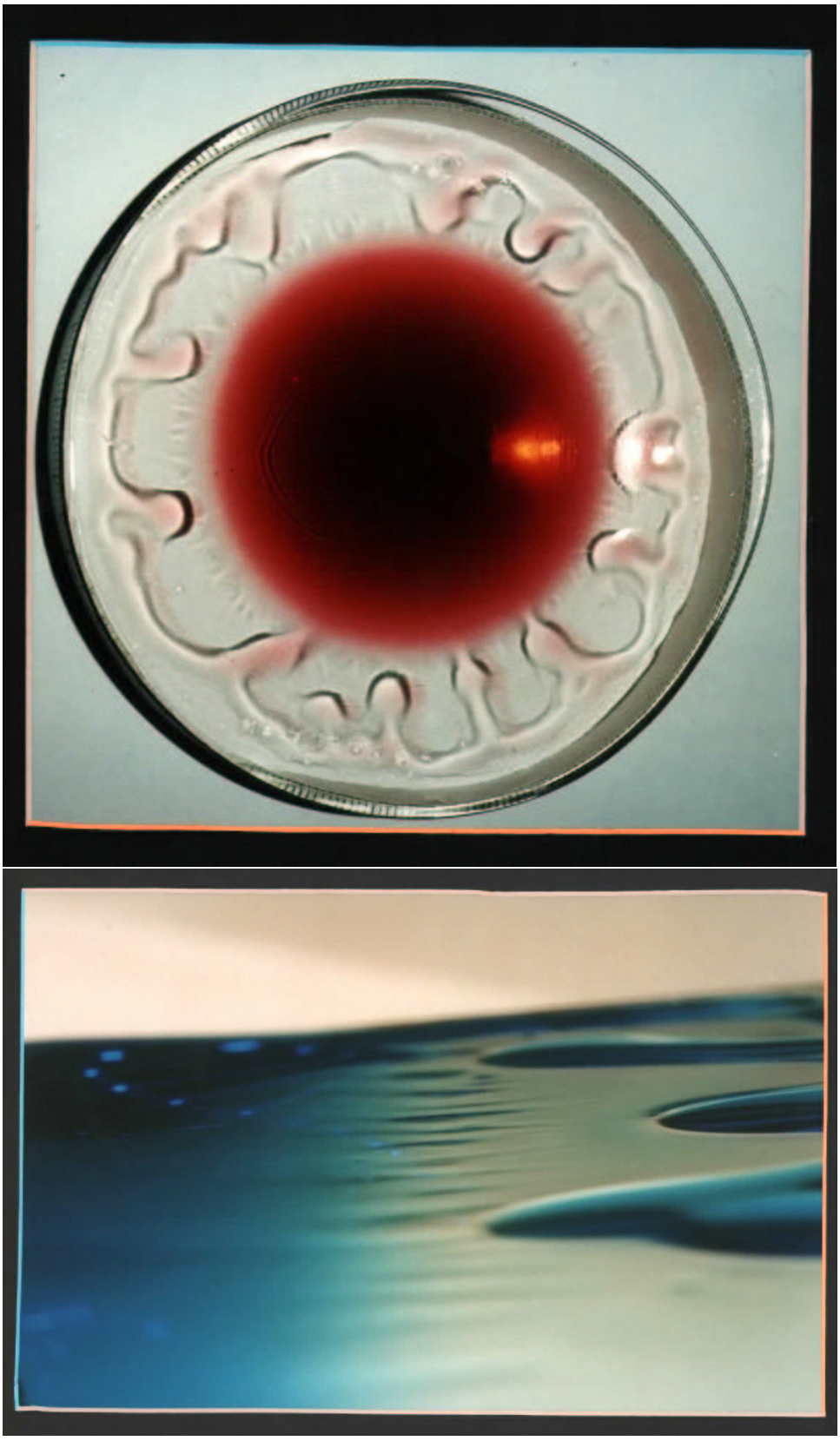

Figure 1.2: Wine ridges and tears shown in a watchglass from above, and on a plate from the side. Photographs courtesy of John Bush's website, http://www-math.mit.edu/ bush/tears.html

Chapter 2

Models

This chapter presents and discusses the important aspects of the ridge-coarsening model developed by Hosoi and Bush [8]. Their model results in a non-linear, fourth-order partial differential equation describing the evolution of the height of the ridges through time.

Also presented in this section is an alternative and more generalized model of ridge development and coarsening using the general thin-film equation as presented in the thin-film survey article by Oron et al. [9] and the simple assumption that surface tension varies linearly with the height of the film.

All of the variables and constants used in these models and throughout the paper are shown in Tables 2.1 and 2.2.

Variable	Symbol	CGS Units
Fluid velocity	$\mathbf{u} = (u, v, w)$	$cm \cdot s^{-1}$
Distance	$\mathbf{x} = (x, y, z)$	cm
Time	t	s
Film height	h	cm
Pressure	p	$g \cdot cm^{-1} \cdot s^{-2}$
Surface Tension	σ	$g \cdot s^{-2}$
Alcohol concentration	c	unitless

Table 2.1: Variables used

Constant	Symbol	CGS Units
Vertical length scale, or average film thickness	H	cm
Horizontal length scale	L	cm
Average speed up the plate	U	$cm \cdot s^{-1}$
Diffusivity of alcohol in water	D	$cm^2 \cdot s^{-1}$
Viscosity	μ	$g \cdot cm^{-1} \cdot s^{-1}$
Density	ρ	$g \cdot cm^{-3}$
Surface stress	$\tau = \mu U/H$	$g \cdot cm^{-1} \cdot s^{-2}$
Surface tension of fluid in reservoir	σ_0	$g \cdot s^{-2}$
Concentration of alcohol in reservoir	c_0	unitless
Change in surface tension due to concentration	α	$g \cdot s^{-2}$
Change in surface tension due to height	β	$g \cdot cm^{-1} \cdot s^{-2}$
Acceleration due to gravity	$\mathbf{g}$	$cm \cdot s^{-2}$
Angle of inclination of plate	θ	unitless

Table 2.2: Constants used

2.1 The Model of Hosoi and Bush

Because we are considering a thin-film where the horizontal length scale, L, is much larger than the vertical length scale, H, i.e. $H \ll L$, we can apply the thin-film or lubrication approximation to our system. This, combined with the fact that we are dealing with relatively small Reynolds numbers, allows the inertial effects of the system to be ignored, simplifying the Navier-Stokes equations to the following as shown in Hosoi and Bush:

$$\nabla p = \mu \nabla^2 \mathbf{u} + \rho \mathbf{g} \tag{2.1}$$

$$\nabla \cdot \mathbf{u} = 0 \tag{2.2}$$

with free surface boundary conditions of

$$\hat{\mathbf{n}} \cdot \mathbf{T} \cdot \hat{\mathbf{s}} = \nabla_x \sigma \tag{2.3}$$

$$\hat{\mathbf{n}} \cdot \mathbf{T} \cdot \hat{\mathbf{n}} = \sigma \nabla \cdot \hat{\mathbf{n}} \tag{2.4}$$

where $\hat{\mathbf{n}}$ is the unit vector normal to the surface of the film, $\hat{\mathbf{s}}$ is the unit vector tangential to the surface of the film, and $\mathbf{T}$ is the stress tensor.

In many systems, the surface tension, σ, can be assumed to be constant. That is not the case for this system. Bush and Hosoi work from the assumption that surface tension is a linear function of concentration of alcohol in the mixture, c,

$$\sigma(c) = \sigma_0 - \alpha(c - c_0) \tag{2.5}$$

where $\alpha = -(\partial\sigma/\partial c)|_{c=c_0}$ and c_0 is the concentration of alcohol in the reservoir. Since the surface tension of water is higher than that of alcohol, surface tension of our mixture decreases as alcohol concentration increases, meaning that α is positive.

Hosoi and Bush derive the following equation for concentration as a function of z, y and h,

$$c = -\frac{\tau}{\alpha} y - \frac{\tau}{\alpha D \mu}\left[\rho g \sin\theta \left(\frac{1}{24} z^4 - \frac{1}{6} h z^3\right) + \frac{1}{6}\tau z^3\right] + c_0 \tag{2.6}$$

and show that when $\mathcal{L}\sin\theta < 1$, (where $\mathcal{L}$ is a nondimensional quantity defined in Table 2.3) concentration is inversely proportional to height. That is, as height increases concentration decreases, leading to increased surface tension and the formation of instabilities. This is the mechanism driving our Marangoni instabilities.

To simplify Equations 2.1 through 2.4, Hosoi and Bush use the functional dependence of σ in Equations 2.5 and 2.6, rescale all of the variables so that they are unitless, apply the lubrication approximation again, and also neglect derivatives in the slowly varying y-direction up the plate.

The variables are rescaled as follows

$$\begin{aligned} (u, v) &= U(\tilde{u}, \tilde{v}) \qquad & w &= \epsilon U \tilde{w} \\ (x, y) &= L(\tilde{x}, \tilde{y}) \qquad & z &= H\tilde{z} \\ p &= (U\mu/H)\tilde{p} \qquad & t &= [H/(U\epsilon^2)]\tilde{t} \end{aligned} \tag{2.7}$$

and the resulting equations for velocity and pressure from Equations 2.1 through 2.4 are solved to a first-order approximation and then averaged across the depth of the film to result in a fourth-order, non-linear partial differential equation for the height of the film along the plate,

$$h_t + \left[\frac{1}{3}h^3(\mathcal{C}h_{xxx} - \mathcal{L}\cos\theta h_x) + \frac{1}{4}\mathcal{M}h^4 h_x(1 - \mathcal{L}h\sin\theta)\right]_x = 0 \tag{2.8}$$

The first term in the brackets represents stabilizing capillarity, the second is a stabilizing gravity term, the third is the destabilizing Marangoni surface stress and the fourth is another stabilizing term due to gravity's effect on the Marangoni convection. This equation is used as a starting point for the rest of the paper.

All of the variables in Equation 2.8 are the non-dimensional versions of the dimensional variables shown in Table 2.1 and are scaled as shown in Equations 2.7. The constants in this equation are non-dimensional quantities as defined in Table 2.3

Dimensionless Quantity	Symbol	Definition
Marangoni numbers	$\mathcal{M}$	$\frac{\tau H^2}{D\mu}$
	$\mathcal{L}$	$\frac{H\rho g}{\tau}$
Capillary number	$\mathcal{C}$	$\epsilon^2\frac{\sigma_0}{\mu U}$
Aspect ratio	ϵ	$\frac{H}{L}$

Table 2.3: Dimensionless quantities

2.2 A More Generalized Approach

Let us instead examine the generalized lubrication model, in one dimension, with a no-slip condition at the fluid-plate interface, and no other external forces besides gravity. From Oron, this becomes

$$\mu h_t + \left[\sigma_x \frac{h^2}{2}\right]_x - \left[\frac{1}{3}h^3(\rho g h \cos\theta - \sigma h_{xx})_x\right]_x = 0 \tag{2.9}$$

To simplify Hosoi and Bush's derivation, and to express it in more generalized terms, we conveniently suppose that our surface tension is not a function of concentration, but rather that it is a linear function of height,

$$\sigma(h) = \sigma_0 + \beta(h - H)$$

where $\beta = (\partial\sigma/\partial h)|_{h=H}$ and H is the thickness of the non-perturbed film. This means that for $\beta > 0$, our surface tension increases with height.

In fact, for this system, σ is *not* a linear function of height. It depends on height in a more complicated fashion as seen in Equations 2.5 and 2.6, but by approximating the dependence as linear, we greatly simplify the derivation of the governing partial differential equation. The approximation may, in fact, work well enough.

Using Equations 2.5 and 2.6, we can actually calculate what β should be for this system

$$\begin{aligned}
\beta &= \left(\frac{\partial\sigma}{\partial h}\right)_{h=H} \\
\beta &= \left(\frac{\partial\sigma}{\partial c}\right)_{c=c_0}\left(\frac{\partial c}{\partial h}\right)_{h=H} \\
\beta &= -\alpha\left(\frac{\tau H^2}{2\alpha D\mu}(\rho g H\sin\theta - \tau)\right) \\
\beta &= \frac{\tau^2 H^2}{2D\mu}\left(1 - \frac{\rho g H}{\tau}\sin\theta\right) \\
\beta &= \frac{\mathcal{M}\tau}{2}(1 - \mathcal{L}\sin\theta)
\end{aligned} \tag{2.10}$$

Returning to Equation 2.9, we rescale the dimensional variables as shown in Equation set 2.7 in order to render the equation dimensionless and simpler to work with.

After completely rescaling our variables, substituting in the calculated value for β from Equation 2.10, and reducing to order ϵ, Equation 2.9 becomes

$$h_t + \left[\frac{1}{3}h^3(\mathcal{C}h_{xxx} - \mathcal{L}\cos\theta h_x) + \frac{1}{4}\mathcal{M}h^2h_x(1 - \mathcal{L}\sin\theta)\right]_x = 0 \tag{2.11}$$

which is essentially the same that was achieved after the lengthy derivation presented in Hosoi and Bush. The difference is that the there are fewer h's in the Marangoni terms. This is a result of approximating surface tension as a linear function of height when in fact it has a higher order dependence.

An advantage to directly deriving a partial differential equation for the evolution of the ridges from the thin-film equations under the assumption that surface tension is a function of height is that this method may be able to be used in other contexts. For example, a thin-film of oil when heated will, under certain conditions, form temperature-driven Marangoni surface instabilities. This could be understood as resulting from the surface tension's dependence on the height of the film. Thicker portions of the film are further from the heat source, thus having a lower temperature and higher surface tension.

Chapter 3

Analysis

Before solving Equation 2.8 numerically, we first apply some analytic techniques to further understand the system. We begin by rewriting the equation as:

$$h_t = -\left[h^3\left(\frac{\mathcal{C}}{3}h_{xx} + f(h)\right)_x\right]_x \tag{3.1}$$

which itself can be rewritten as

$$h_t = -\left[h^3 f'(h)h_x\right]_x + \mathcal{O}(h_{xxxx}) \tag{3.2}$$

where

$$f(h) = -\frac{1}{12}\mathcal{M}L\sin\theta h^3 + \frac{1}{8}\mathcal{M}h^2 - \frac{1}{3}\mathcal{L}\cos\theta h \tag{3.3}$$

$$f'(h) = -\frac{1}{4}\mathcal{M}\mathcal{L}\sin\theta h^2 + \frac{1}{4}\mathcal{M}h - \frac{1}{3}\mathcal{L}\cos\theta \tag{3.4}$$

Ignoring the $\mathcal{O}(h_{xxxx})$ terms of Equation 3.2, we see that in order to avoid destabilizing negative diffusion, we must have $h^3 f'(h) \leq 0$. The height of the fluid, h, is always positive, so the stability is governed by the sign of $f'(h)$, which is a parabola opening downward.

Our two roots are given by

$$r_1, r_2 = \mathcal{M}\left(\frac{1 \mp \sqrt{1 - \frac{16}{3\mathcal{M}}\mathcal{L}^2\sin\theta\cos\theta}}{2\mathcal{L}\sin\theta}\right) \tag{3.5}$$

Since $0 < \theta < \frac{\pi}{2}$ and $\mathcal{M}, \mathcal{L} > 0$, we see that $\frac{16}{3\mathcal{M}}\mathcal{L}^2\sin\theta\cos\theta > 0$, meaning we cannot have a negative root. This makes sense because otherwise no thin-film would be stable.

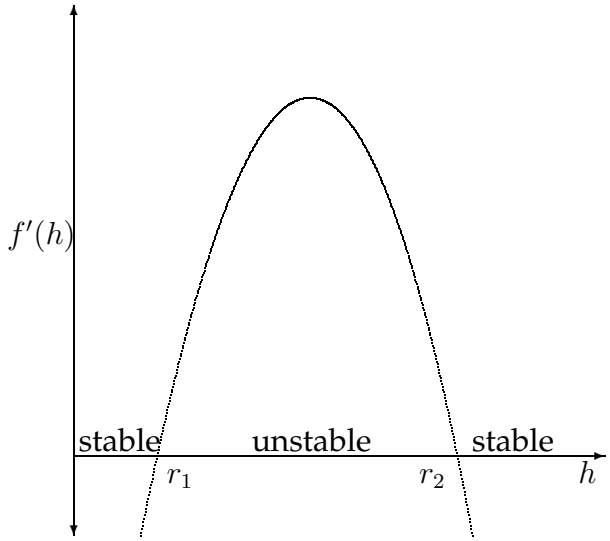

Figure 3.1: Stability graph

Given the physical parameters, we know that $\frac{16}{3\mathcal{M}}\mathcal{L}^2 \sin\theta\cos\theta < 1$, so both roots are real, giving us two positive roots, r_1 and r_2 as shown in Figure 3.1

This can give us an understanding as to why the ridges form. When $r_1 < h < r_2$, $f'(h) > 0$, meaning the surface is unstable and will adjust until $h < r_1$ or $h > r_2$. The smaller positive root corresponds to the maximum stable height of the thin-film connecting the ridges. The larger positive root corresponds to the minimum height a stable ridge can be. When $f'(h) > 0$, we have negative diffusion and the fluid surface is unstable.

3.1 Linear Stability Analysis

A linear stability analysis can be conducted on Equations 2.8 and 2.11 as is done in Hosoi and Bush. To gain further insight, we examine what happens when we let $h = 1 + \bar{h}$, where $\bar{h}$ is a very small perturbation around the base height of $H = 1$. That is, we are seeing what happens when we slightly perturb the steady, level fluid. This technique allows us to ignore the non-linear effects.

Substituting this linearized h into both 2.8 and 2.11 yields the same linear partial differential equation,

$$\bar{h}_t + \left[\frac{1}{4}\mathcal{M}(1 - \mathcal{L}\sin\theta) - \frac{1}{3}\mathcal{L}\cos\theta\right]\bar{h}_{xx} + \frac{1}{3}\mathcal{C}\bar{h}_{xxxx} = 0 \tag{3.6}$$

which means that if we look for wave solutions to Equations 2.8 and 2.11 of the form $\bar{h}(x) = e^{\omega t}e^{ikx}$ where ω is the growth rate of the solution and k is the wavenumber, we find the dispersion relation between ω and k to be

$$\omega = \left[\frac{1}{4}\mathcal{M}(1 - \mathcal{L}\sin\theta) - \frac{1}{3}\mathcal{L}\cos\theta\right]k^2 - \frac{1}{3}\mathcal{C}k^4 \tag{3.7}$$

When $\omega < 0$, perturbations decay in time and the solution is stable. Conversely, the solution is unstable and ridges form when $\omega > 0$ or

$$\frac{1}{3}\mathcal{L}\cos\theta < \frac{1}{4}\mathcal{M}(1 - \mathcal{L}\sin\theta) \tag{3.8}$$

If this condition holds, then perturbations are magnified, forming ridges. The most unstable wavelength occurs when ω is maximized, which happens when $\frac{\partial\omega}{\partial k} = 0$. We see that the most unstable wave number is

$$k_* = \sqrt{\left[\frac{3}{8}\mathcal{M}(1 - \mathcal{L}\sin\theta) - \frac{1}{2}\mathcal{L}\cos\theta\right]/\mathcal{C}} \tag{3.9}$$

where $k_* = \frac{2\pi}{\lambda_*}$, λ_* being the unitless wavelength of the ridges. So $k_{exp} = k_*/(2\pi)$ is the number of ridges we expect to initially arise from random initial conditions in a unitless interval of length 1 before the non-linear Marangoni effects cause coarsening to occur. Table 3.1 shows the expected and observed wave numbers for a variety of different runs.

Run	$\mathcal{C}$	$\mathcal{L}$	$\mathcal{M}$	θ	k_{exp}	k_{obs}
H9	0.01	2	500	0.45	7.71	8
H10	0.01	2	900	0.45	10.44	10
H23	0.1	3	500	0.2	4.33	5
H2c	0.005	2.1	200	0.45	5.30	5

Table 3.1: Expected and observed wave numbers for various runs

3.2 Steady State Ridge Profile

In the system, the ridges eventually stop coarsening and become relatively stable. This also occurs in the two numerical models developed and discussed in Chapter 4. We can examine the shape and size of the steady-state ridges by examining what occurs when we let $h_t = 0$. From Equation 3.1 we see that in order for this to occur

$$\frac{\mathcal{C}}{3}h_{xx} + f(h) = P \tag{3.10}$$

where P is a constant, pressure-like term. The mature, quasi-steady-state ridges shown in Figure 4.5 have relatively constant P terms within the ridges, supporting this claim. Multiplying both sides of equation 3.10 by h_x and integrating with respect to x we get that

$$\frac{\mathcal{C}}{6}h_x^2 - \frac{1}{48}\mathcal{ML}\sin\theta h^4 + \frac{1}{24}\mathcal{M}h^3 - \frac{1}{6}L\cos\theta h^2 + K = Ph$$
$$h_x^2 = \frac{1}{8\mathcal{C}}\left(\mathcal{ML}\sin\theta h^4 - 2\mathcal{M}h^3 + 8\mathcal{L}\cos\theta h^2 + 48Ph + K\right)$$

where K is a constant of integration. This leads to an ordinary differential equation for the height of a constant-P, non-evolving ridge,

$$h_x = \pm\sqrt{\frac{1}{8\mathcal{C}}\left(\mathcal{ML}\sin\theta h^4 - 2\mathcal{M}h^3 + 8\mathcal{L}\cos\theta h^2 + 48Ph + K\right)} \tag{3.11}$$

If the values of $\mathcal{C}$, $\mathcal{L}$, $\mathcal{M}$, and θ, our non-dimensional parameters, P, our steady-state pressure within the ridge, and K, the constant of integration, are all known

then Equation 3.11 can be solved using a fourth-order Runge-Kutta method.

The parameters of $\mathcal{C} = 0.1, \mathcal{L} = 3, \mathcal{M} = 500$ and $\theta = 0.2$ are used because the corresponding numerical simulation for run H23 is well-behaved, reaches a quasi-steady-state solution, and produces a nice number of ridges.

These parameters were used in the numerics of Chapter 4 to evolve an initial random profile into four steady-state ridges shown in figure 4.5. Both numerical methods produced ridges with a relatively constant value of about $P = 33$ within them. Using these parameters, along with setting $K = 0$, Equation 3.11 is solved using a fourth-order Runge-Kutta method. The positive square root was used to produce the left side of the ridge, and the negative square root was used to produce the right side of the ridge. The results can be seen in Figure 3.2.

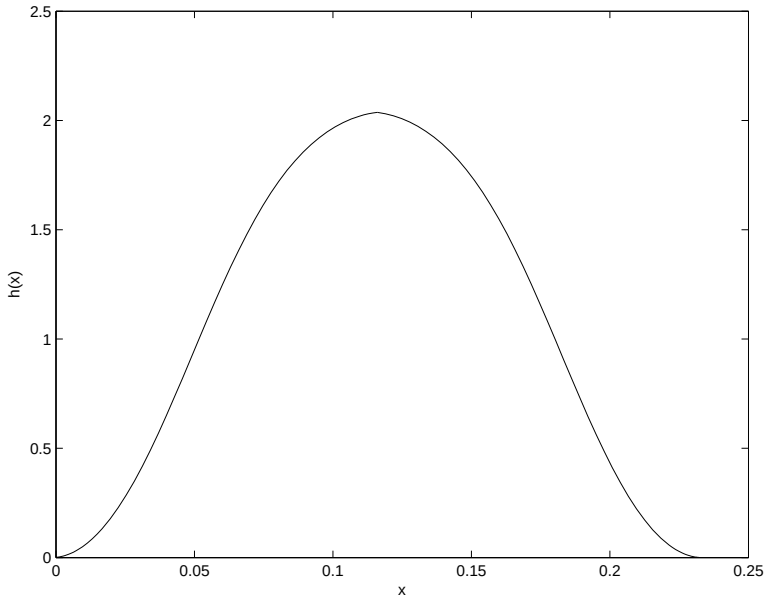

Figure 3.2: Constant pressure ridge for run H23 parameters

Notice the nearly identical size and shape as the ridges produced in Figure 4.5. This could possibly lead to the development of a relationship between the pressure and size and shape of the resulting ridge.

Some of the numerical results from Chapter 4 show the larger ridges interspersed with smaller ridges as shown in Figure 3.2. These smaller ridges have their own smaller, constant pressure term. Since these ridges are occurring when

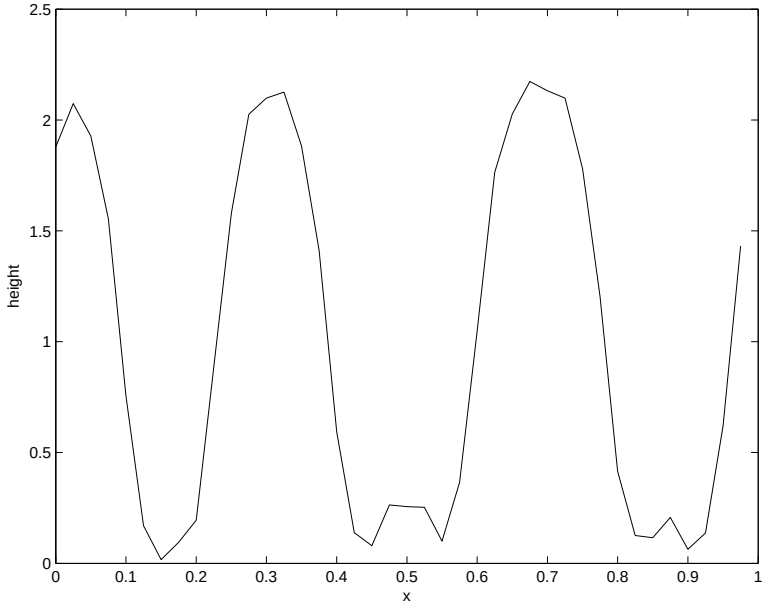

Figure 3.3: Large ridges interspersed with smaller ones

the height, h, is small, the h^2, h^3, and h^4 terms of equation 3.11 could possibly be ignored to produce parabolas. This has not yet been examined in any depth.

Chapter 4

Numerical Models

Two distinct but complementary numerical models were programmed using Matlab to solve Equation 2.8 on an interval with random perturbations around the base height of $H = 1$ and periodic boundary conditions. The first model uses a centered finite-difference scheme for calculating spatial derivatives with an implicit timestep. The second model uses a pseudospectral method for spatial derivatives and takes an explicit time step, but at every timestep the solution is integrated to within an acceptable error using a fourth-order Runge-Kutta integrator. The two major differences in these two methods, and in most numerical methods in general, are how the spatial and time derivatives are treated. This chapter will briefly explore some of these issues and see how they apply to our system in particular.

4.1 Time Derivatives: Explicit versus Implicit

Looking at Equation 2.8 we see that the time derivative of h is a function of the spatial derivatives and the dimensionless parameters,

$$\frac{\partial h}{\partial t} = f(h^n, h_x^n, h_{xx}^n, \ldots, \text{parameters}) \tag{4.1}$$

If h_i^n is the height of the film at node i and time n, and Δt is the size of our timestep, then the time derivative of h at node i can be approximated as

$$\frac{\partial h_i}{\partial t} \approx \frac{h_i^{n+1} - h_i^n}{\Delta t} \tag{4.2}$$

An explicit time step sets the time derivative equal to f evaluated at the *current*

timestep,

$$\frac{h^{n+1} - h^n}{\Delta t} = f(h^n, h_x^n, h_{xx}^n, \ldots, \text{parameters})$$

To advance the solution forward one timestep, we simply use the known solution at the current time to individually advance each point. This is fairly straightforward to solve, but often either entirely unstable or requiring extremely small timesteps.

An implicit time step sets the time derivative equal to f evaluated at the *next* timestep,

$$\frac{h^{n+1} - h^n}{\Delta t} = f(h^{n+1}, h_x^{n+1}, h_{xx}^{n+1}, \ldots, \text{parameters})$$

This involves advancing all the points forward one timestep simultaneously. So each timestep involves inverting an N by N sized matrix, where N is the number of points in our solution. This method is always stable but much more computationally intensive to solve than the explicit timestep. An implicit timestep was used in the finite-difference model. An explicit timestep was used with the pseudospectral method, but to maintain stability a fourth-order Runge-Kutta method with an adaptive timestep was used to integrate the solution at each timestep to within an acceptable error range.

4.2 Spatial Derivatives: Finite Differences versus Pseudospectral

The difficulty in solving equations numerically is that we must discretize what is a continuous system. This creates problems in how derivatives are taken. There are several different possible approaches when trying to approximate spatial derivatives. In general terms, however, we are always simply just linearly recombining our nodal values at each point in the solution interval to calculate the derivative at each point. So calculating the derivatives becomes equivalent to multiplying our

solution vector by a "derivative matrix" D, where

$$f_x = Df \qquad f_{xx} = D^2 f \qquad f_{xxx} = D^3 f \qquad f_{xxxx} = D^4 f \tag{4.3}$$

The question then becomes what to use for our derivative matrix of weights, D.

The most straight-forward and intuitive approach for calculating derivatives is the centered finite-difference method. To calculate a spatial derivative of our function f at node i, we simply calculate a rate of change between the two immediate neighbors,

$$\frac{\partial f_i}{\partial x} = \frac{f_{i+1} - f_{i-1}}{2\Delta x} \tag{4.4}$$

where Δx is the size of our grid spacing. For example, if we have a length $L = 1$ interval with $J = 10$ nodes, $\Delta x = 0.1$, and the finite-difference approach gives us a derivative matrix

$$D = \begin{bmatrix} 0 & 5 & 0 & 0 & 0 & 0 & 0 & 0 & 0 & -5 \\ -5 & 0 & 5 & 0 & 0 & 0 & 0 & 0 & 0 & 0 \\ 0 & -5 & 0 & 5 & 0 & 0 & 0 & 0 & 0 & 0 \\ 0 & 0 & -5 & 0 & 5 & 0 & 0 & 0 & 0 & 0 \\ 0 & 0 & 0 & -5 & 0 & 5 & 0 & 0 & 0 & 0 \\ 0 & 0 & 0 & 0 & -5 & 0 & 5 & 0 & 0 & 0 \\ 0 & 0 & 0 & 0 & 0 & -5 & 0 & 5 & 0 & 0 \\ 0 & 0 & 0 & 0 & 0 & 0 & -5 & 0 & 5 & 0 \\ 0 & 0 & 0 & 0 & 0 & 0 & 0 & -5 & 0 & 5 \\ 5 & 0 & 0 & 0 & 0 & 0 & 0 & 0 & -5 & 0 \end{bmatrix}$$

A more involved global approach to taking spatial derivatives for functions on periodic intervals such as the one we are dealing with in our system is the pseudospectral approach. Let's say that we divide our length L interval into J nodes. In the finite-difference approach, we only use the information contained in 2 of these J nodes for calculating the derivative. The pseudospectral method uses

the fact that our function is periodic on our interval and can be represented as a partial Fourier series of sines and cosines. The derivation shown in Appendix A shows that our matrix of weights, D, for the pseudospectral method becomes,

$$D_{jk} = \begin{cases} 0 & \text{if } j = k, \\ \frac{\pi}{L} \cos(j-k)\pi \cot \frac{(j-k)\pi}{J} & \text{if } j \neq k. \end{cases} \tag{4.5}$$

For our example interval with $L = 1$ and $J = 10$ the pseudospectral method gives us the derivative matrix

$$D = \begin{bmatrix} 0 & 9.7 & -4.3 & 2.3 & -1.0 & 0 & 1.0 & -2.3 & 4.3 & -9.7 \\ -9.7 & 0 & 9.7 & -4.3 & 2.3 & -1.0 & 0 & 1.0 & -2.3 & 4.3 \\ 4.3 & -9.7 & 0 & 9.7 & -4.3 & 2.3 & -1.0 & 0 & 1.0 & -2.3 \\ -2.3 & 4.3 & -9.7 & 0 & 9.7 & -4.3 & 2.3 & -1.0 & 0 & 1.0 \\ 1.0 & -2.3 & 4.3 & -9.7 & 0 & 9.7 & -4.3 & 2.3 & -1.0 & 0 \\ 0 & 1.0 & -2.3 & 4.3 & -9.7 & 0 & 9.7 & -4.3 & 2.3 & -1.0 \\ -1.0 & 0 & 1.0 & -2.3 & 4.3 & -9.7 & 0 & 9.7 & -4.3 & 2.3 \\ 2.3 & -1.0 & 0 & 1.0 & -2.3 & 4.3 & -9.7 & 0 & 9.7 & -4.3 \\ -4.3 & 2.3 & -1.0 & 0 & 1.0 & -2.3 & 4.3 & -9.7 & 0 & 9.7 \\ 9.7 & -4.3 & 2.3 & -1.0 & 0 & 1.0 & -2.3 & 4.3 & -9.7 & 0 \end{bmatrix}$$

which is an obvious contrast to the sparse derivative matrix used in the finite-difference scheme. Here, *all* of the points in the interval are used in calculating the derivative at a point, not just the two immediate neighboring points.

The pseudospectral method is very efficient and accurate for calculating the derivatives of periodic functions, like the $\sin$ function shown in Figure 4.1.

However, the pseudospectral method becomes much less efficient for calculating derivatives for functions which are not easily represented as a partial Fourier series of sines and cosines, like the step function shown in Figure 4.2.

As might be expected in modeling the ridge formation and evolution, because the ridges are very periodic, the pseudospectral method does a good job approx-

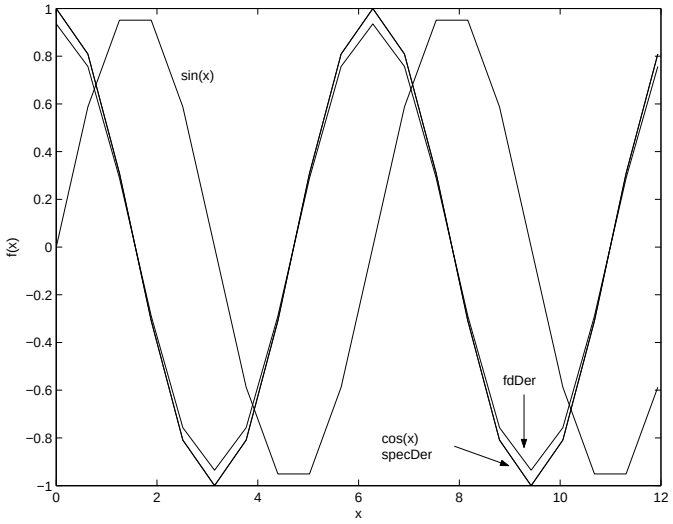

Figure 4.1: Plots of $\sin x$,$\cos x$ and the derivative of $\sin x$ taken using both pseudospectral and finite-differencing. The pseudospectral derivative and $\cos x$ lie directly on top of each other, showing the high accuracy pseudospectral derivatives have for periodic functions. The finite-difference derivative, however, is clearly much less accurate in this situation.

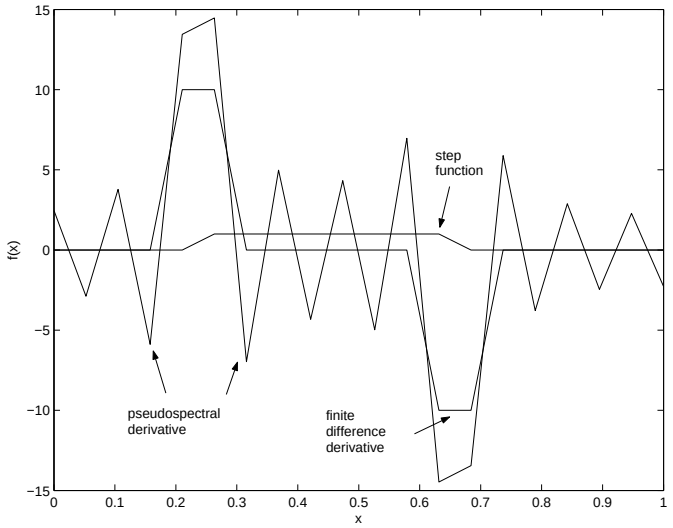

Figure 4.2: A step function and its pseudospectral and finite-difference derivatives. Because the step function does not lend itself to being easily represented by sines and cosines in a partial Fourier series, the finite-difference method of taking derivatives is much more accurate.

imating spatial derivatives. We can, in fact, use far fewer grid points with the pseudospectral method to achieve the same order of accuracy achieved using the finite-difference approach.

4.3 Numerical Results

Both the pseudospectral and finite-difference methods were tested for a variety of parameters as shown in Appendix B. In all cases we began with some random perturbation around the base height of $H = 1$. For parameter sets that were stable according to Equation 3.8, no ridges formed. However, for unstable parameter sets both numerical models successfully simulated the formation and evolution of the ridges. In most cases the initial wavelength seen to emerge before any coarsening occurred was correctly predicted by Equation 3.9. In many cases, coarsening was observed for both methods and can be seen in the Figures 4.3 and 4.4. Figure 4.5 shows the quasi-steady-state ridges and the nearly-constant pressure-term profiles for both numerical methods using certain parameters.

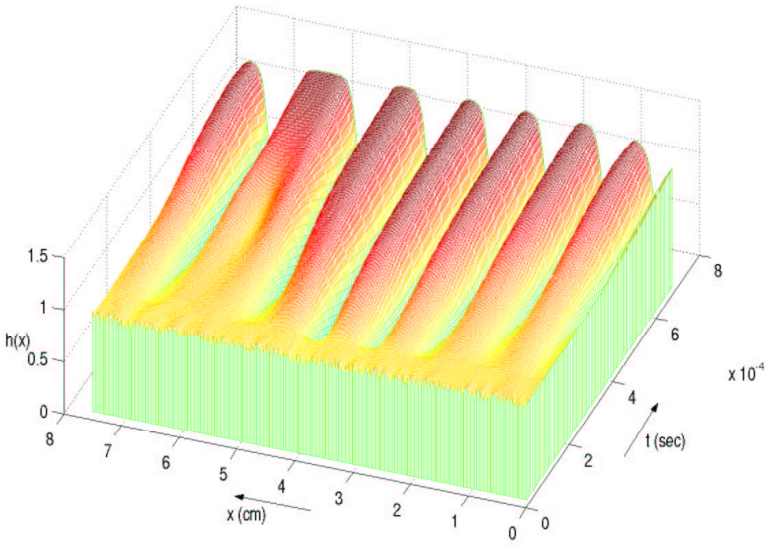

(a) Run H9: finite-difference method using 334 grid points

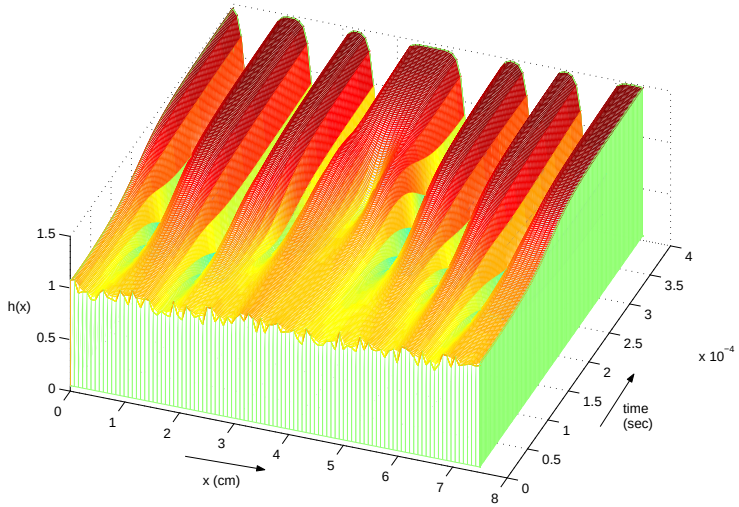

(b) Run H9s: pseudospectral method using 100 grid points

Figure 4.3: Ridge evolution and coarsening for both methods solving Equation 2.8. Parameters used were $\mathcal{C} = .01, \mathcal{L} = 2, \mathcal{M} = 500, \theta = .45, H = 0.003$ cm and $L = 7.5$ cm.

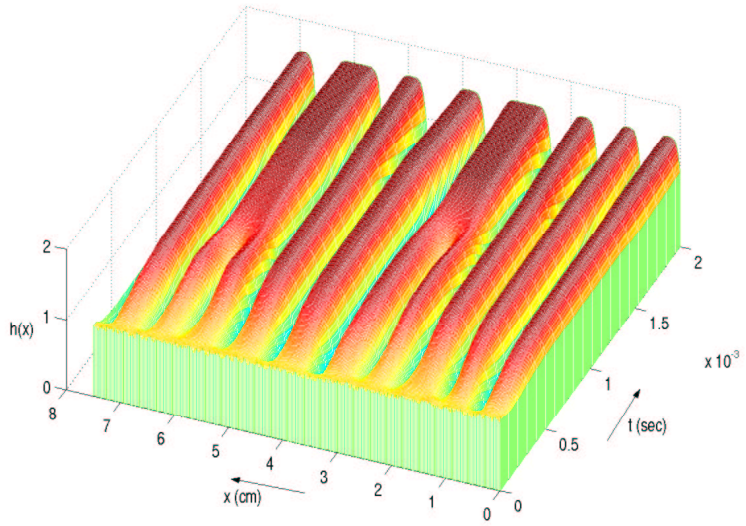

(a) Run H10: finite-difference method using 334 grid points

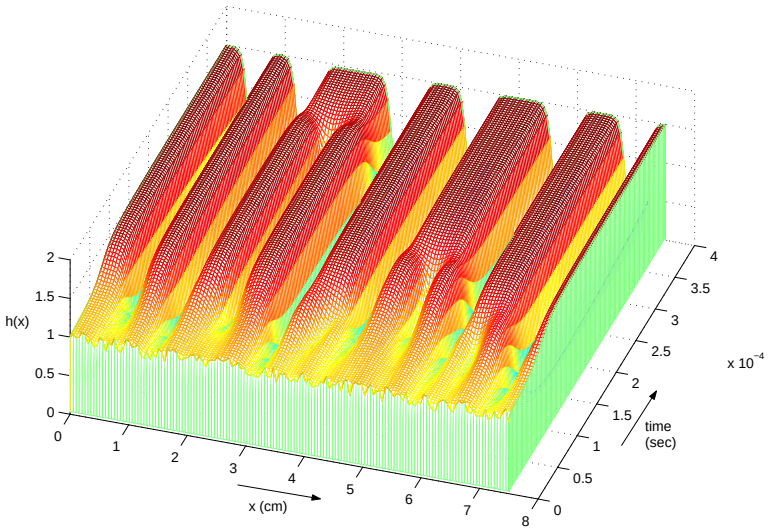

(b) Run H10s: pseudospectral method using 150 grid points

Figure 4.4: Ridge evolution and coarsening for both methods solving Equation 2.8. Parameters used were $\mathcal{C} = .01, \mathcal{L} = 2, \mathcal{M} = 900, \theta = .45, H = 0.003$ cm and $L = 7.5$ cm.

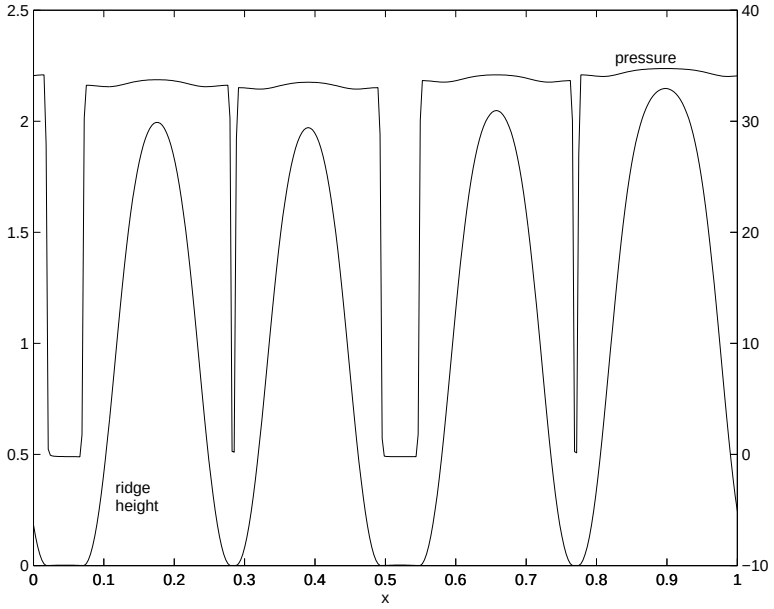

(a) Run H23: finite-difference method using 334 grid points

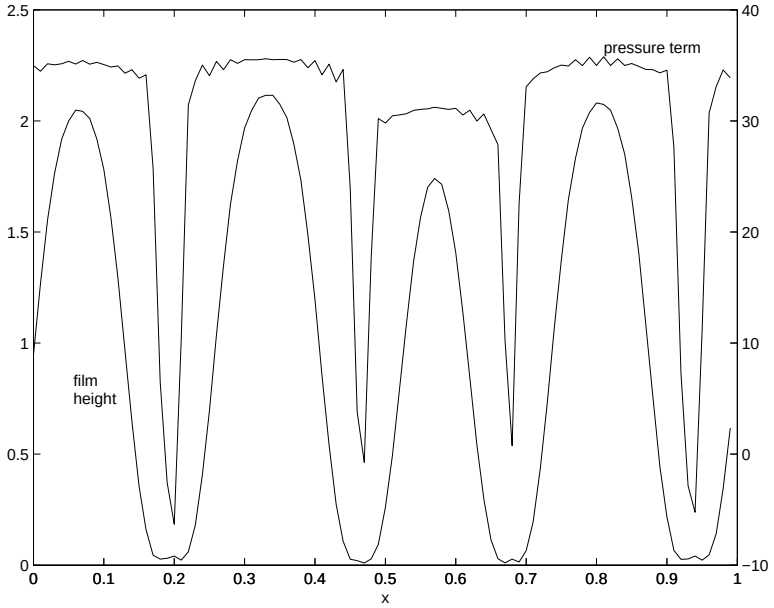

(b) Run H23s: pseudospectral method with 100 grid points

Figure 4.5: Steady-state ridges and their nearly constant pressures for $\mathcal{C} = .1, \mathcal{L} = 3, \mathcal{M} = 500, \theta = .2, H = 0.003$ cm and $L = 7.5$ cm.

4.4 Positivity Issues

Both of the numerical methods worked well for solving Equation 2.8 in the initial timesteps. As long as the parameters used caused the system to be unstable, ridges would develop. However, virtually all of the simulations had problems with eventually returning negative values and developing singularities. Once this occurred, the solution could no longer be solved for future timesteps. Numerous attempts were made to try to fix the negativity problems.

For the finite-difference method, a positivity-preserving scheme presented in the paper by Zhornitskaya and Bertozzi [11] was implemented in the attempt to avoid physically impossible negative values and the resulting singularities. This scheme changed the way the h^3 in front of the Ch_{xxx} term was approximated. This positivity preserving scheme helped, but did not entirely get rid of solutions becoming negative.

The same negativity problems were found with the pseudospectral method as well. This problem of obtaining negative, singular solutions still remains unresolved.

Chapter 5

Conclusion and Future Work

Surface instabilities in thin-film mixtures of alcohol and water, like wine swirled up on the inside of a glass, driven by Maragoni convection, leads to a variety of different and interesting mathematics. In the paper on this topic by Hosoi and Bush [8], the lubrication approximation and various other simplifications are used to reduce the Navier-Stokes equations to a single, one-dimensional, non-linear partial differential equation describing the evolution of the height of the film in time. The majority of the work done was from this equation.

A more generalized approach was taken, using the simplifying assumption that surface tension is merely a linear function of height. This assumption was used with the general thin-film equation as presented in Oron [9] to derive an alternative partial differential equation for the height of the film. This partial differential equation is exactly the same as Hosoi and Bush's except that the non-linear Marangoni terms have a lower order dependence upon h.

A variety of analytical techniques were used to gain more insight into the development of the ridges. A linear stability analysis was done on both Equations 2.8 and 2.11 to predict the most unstable ridge wavelength that will intially emerge before non-linear effects cause coarsening to occur. To this linear approximation, both equations are the same, and the number of initial emerging ridges predicted by this analysis was accurate for the majority of numerical simulations.

The majority of the work accomplished was numerically solving Equation 2.8. It was successfully solved using two different methods. The first method used was a centered finite-difference approach with an implicit timestep. The second

method used a pseudospectral scheme to calculate spatial derivatives and took explicit timesteps which were adapted appropriately by a fourth order Runge-Kutta solver to within an acceptable error range. Both of these methods were relatively successful in numerically solving this non-linear partial differential equation and modeling the ridge emergence and coarsening. Yet both solvers had problems with preserving positivity.

Future work would be to try making the solvers more numerically robust and avoid negative values and singularities. Also, further development of the more generalized model resulting in Equation 2.11 would be interesting. It was shown in this paper that to a linear approximation, this newly derived equation is identical to Equation 2.8 derived by Hosoi and Bush. What is not known is how the different non-linear Marangoni terms effect the coarsening dynamics of the ridges. It may be that the physical differences that result are essentially negligible, but it also may be true that these differences significantly effect the coarsening dynamics. Solving Equation 2.11 numerically and comparing the results with Hosoi and Bush's equation solved with the same parameters could answer these questions.

Appendix A

Derivation of the Pseudospectral Derivative Matrix

Assume that we have a function $f(x)$ periodic on an interval of length L whose nodal values, f_k are known at J equally spaced points on the interval. We know that the f can be approximated as the partial Fourier series

$$f(x) \approx \sum_{k=0}^{J-1} c_k e^{ikx} \tag{A.1}$$

where c_k are the Fourier coefficients. Multiplying both sides by $e^{-i\tilde{k}x}$ and integrating over our interval we get

$$\begin{aligned}
\int_0^L f(x)e^{-i\tilde{k}x}\ \mathrm{dx} &\approx \int_0^L \sum_{k=0}^{J-1} c_k e^{-i\tilde{k}x} e^{ikx}\ \mathrm{dx} \\
&\approx \int_0^L \left(c_0 e^{-i\tilde{k}x} e^{0ix} + c_1 e^{-i\tilde{k}x} e^{ix} + c_2 e^{-i\tilde{k}x} e^{2ix} + \dots \right)\ \mathrm{dx} \\
&\approx c_0 \int_0^L e^{-i\tilde{k}x} e^{0ix}\ \mathrm{dx} + \mathrm{c}_1 \int_0^L \mathrm{e}^{-\mathrm{i}\tilde{\mathrm{k}}\mathrm{x}} \mathrm{e}^{\mathrm{ix}}\ \mathrm{dx} + \mathrm{c}_2 \int_0^L \mathrm{e}^{-\mathrm{i}\tilde{\mathrm{k}}\mathrm{x}} \mathrm{e}^{2\mathrm{ix}}\ \mathrm{dx} + \dots \\
&\approx L c_{\tilde{k}}
\end{aligned}$$

because

$$\int_0^L e^{-i\tilde{k}x} e^{ix}\ \mathrm{dx} = \begin{cases} 0 & \text{if } k \neq \tilde{k}, \\ L & \text{if } k = \tilde{k}. \end{cases}$$

Therefore,

$$c_k \approx \frac{1}{L} \int_0^L f(\tilde{x}) e^{-ik\tilde{x}}\ \mathrm{d\tilde{x}} \tag{A.2}$$

meaning Equation A.1 becomes

$$\begin{aligned} f(x) &\approx \sum_{k=0}^{J-1} c_k e^{ikx} \\ &\approx \sum_{k=0}^{J-1} \left(\frac{1}{L} \int_0^L f(\tilde{x}) e^{-ik\tilde{x}} \, \mathrm{d}\tilde{\mathrm{x}} \right) e^{ikx} \\ &\approx \sum_{k=0}^{J-1} \int_0^L \left(\frac{1}{L} f(\tilde{x}) e^{ik(x-\tilde{x})} \right) \, \mathrm{d}\tilde{\mathrm{x}} \\ &\approx \sum_{k=0}^{J-1} \sum_{l=0}^{J-1} \frac{1}{J} f_l e^{ik(x-x_l)} \\ &\approx \frac{1}{J} \sum_{l=0}^{J-1} f_l \sum_{k=0}^{J-1} e^{ik(x-x_l)} \\ &\approx \frac{1}{J} \sum_{l=0}^{J-1} f_l \sum_{k=0}^{J-1} r^k \end{aligned}$$

where $r = e^{i(x-x_l)}$. If $S = \sum_{k=0}^{J-1} r^k$ then

$$\begin{aligned} S &= r^0 + r^1 + r^2 + \cdots + r^{J-1} \\ rS &= r^1 + r^2 + \cdots + r^J \\ S - rS &= r^0 - r^J = 1 - r^J \\ S &= \frac{1 - r^J}{1 - r} = \frac{1 - e^{iJ(x-x_l)}}{1 - e^{i(x-x_l)}} \end{aligned}$$

which, expanded out, becomes

$$S_l(x) = \frac{1}{J} \sin \frac{J(x - x_l)}{2} \cot \frac{(x - x_l)}{2} \tag{A.3}$$

giving us that

$$f(x) \approx \frac{1}{J} \sum_{l=0}^{J-1} S_l(x) f_l \tag{A.4}$$

and

$$f'(x) \approx \sum_{l=0}^{J-1} S_l'(x) f_l \tag{A.5}$$

Taking the derivative of $S_l(x)$ with respect to x gives us our pseudospectral derivative matrix D,

$$D_{jk} = \begin{cases} 0 & \text{if } j = k, \\ \frac{\pi}{L} \cos{(j-k)\pi} \cot{\frac{(j-k)\pi}{J}} & \text{if } j \neq k. \end{cases} \tag{A.6}$$

Appendix B

Runs Conducted

Name	$\mathcal{C}$	$\mathcal{L}$	$\mathcal{M}$	θ	Approximate height of mature ridges	k_{exp}	Number of observed ridges
Hs	.1	0	200	.45	3-4	4.36	5
H2	.005	2.2	200	.45	-	3.37	2?
H2b	.005	2.3	200	.45	1	0	0
H2c	.005	2.1	200	.45	1.3	5.30	5,3,0
H3	.2	1	200	.45	2.5	2.30	2
H4	.1	1	200	.45	2.5	3.26	3
H5	.2	2	300	.45	1.5	1.32	1
H5b	.2	2	1000	.45	1.5	2.46	2
H5c	.2	2.1	1000	.45	1.5	2.00	2,1
H5d	.4	2	1000	.45	1.5	1.74	2,1
H6s	.02	1	500	.45	2.5	11.56	11,10
H7	.1	1	500	.45	2.5	5.17	5
H8	.01	1	500	.45	2-4	16.35	17,16
H9	.01	2	500	.45	1.5	7.71	8,7,6
H10	.01	2	900	.45	1.5	10.44	10,9,8

Table B.1: Runs using the centered finite difference method with 334 grid points on Equation 2.8. Empty entries means the simulation was not run sufficiently long for the ridges to fully develop. A ridge height of 1 and $k_{exp} = 0$ means that the solution is linearly stable for the given parameters, i.e. $\mathcal{L}\sin\theta > 1$.

Name	$\mathcal{C}$	$\mathcal{L}$	$\mathcal{M}$	θ	Approximate height of mature ridges	k_{exp}	Number of observed ridges
H11	.1	2	900	.45	1.5	3.30	3,2
H12	.01	3	900	.45	1	0	0
H13	.01	2.5	1500	.45	1	0	0
H14	.001	3	1500	.45	1	0	0
H15	.0001	3	1500	.45	1	0	0
H16	.00001	3	1500	.45	1	0	0
H17	.01	3	1500	.45	1	0	0
H18	.001	3	1500	.45	1	0	0
H19	.001	3	1500	.45	1	0	0
H20	.01	2.2	1500	.45	1.5	7.67	7?,3
H21	.02	2.2	1200	.45	1.5	4.83	5?,2
H22	.01	.1	200	.45	3-4.5	13.48	13
H23	.1	3	500	.2	2	4.34	5,4
H24	.1	3	1000	.2	2	6.16	6
H25	.05	3	1000	.2	2	8.72	9,8
H26	.1	4	1000	.2	-	4.36	5
H27	.02	4	1000	.2	-	9.75	10
H28	.01	4	1000	.2	1.7	13.79	12,11,10
H29	.001	9	1000	.1	-	29.17	25?
H30	.005	9	1000	.1	1.5	13.04	13,10
H31	.003	9	1000	.1	1.5	16.84	17,13
H32	.008	15	1300	.05	1.8	19.04	18,17
H33	.008	20	2000	.05	1	0	0
H34	.01	40	2000	.01	-	33.00	30-35?
H35	.1	100	2000	.001	2-5	12.58	13
H36	.07	500	5000	.001	2-2.5	15.77	16,15,14

Table B.2: More centered finite difference runs with 334 grid points

Name	$\mathcal{C}$	$\mathcal{L}$	$\mathcal{M}$	θ	Number of grid points	Approximate height of mature ridges	k_{exp}	Number of observed ridges
H9s	.01	2	500	.45	100	1.5	7.71	7,6
H10s	.01	2	900	.45	150	1.5	10.44	10,8,6
H23s	.1	3	500	.2	100	2	4.34	4
H23bs	.1	3	500	.2	40	2	4.34	4,3
H27	.02	4	1000	.2	100	1.7	9.75	10,8,7

Table B.3: Some runs using the pseudospectral method on Equation 2.8

Bibliography

[1] A. L. Bertozzi, G. Grün, and T. P. Witelski. Dewetting films: bifurcations and concentrations. *Nonlinearity*, 14(6):1569–1592, 2001. Examines a fourth-order lubrication equation similar to ours in which coarsening of droplets occurs.

[2] A. L. Bertozzi and M. C. Pugh. Long-wave instabilities and saturation in thin film equations. *Comm. Pure Appl. Math.*, 51(6):625–661, 1998. Another analytic approach to a similar unstable thin-film equation.

[3] T. E. Faber. *Fluid dynamics for physicists*. Cambridge University Press, Cambridge, 1997. A great introduction to fluid dynamics.

[4] X. Fanton and A. M. Cazabat. Spreading and instabilitites induced by a solutal marangoni effect. *Langmuir*, 14(9):2554–2561, 1998. A description of some experimental results measuring coarsening rate, ridge drift velocity and other things for a variety of alcohol and water mixtures. May possibly be able to use some of these measurements in addition to my own.

[5] C. A. J. Fletcher. *Computational techniques for fluid dynamics. 1*. Springer Series in Computational Physics. Springer-Verlag, Berlin, 1988. Describes the common numerical techniques used in fluid dynamics including the centered finite-difference and pseudospectral methods. Useful reference.

[6] J. B. Fournier and A. M. Cazabat. Tears of wine. *Europhys. Lett.*, 20(6):517–522, 1992. An earlier paper describing the ”tears of wine” phenomena and presents some preliminary measurements for the tears and ridges.

[7] K. B. Glasner and T. P. Witelski. Coarsening dynamics of dewetting films. *preprint*, May 2002. Along the same lines as the Bertozzi papers, but it is easier to understand and some of the analysis is more applicable. They simplify their non-linear PDE as a system of ODE's describing the pressure and position for the bumps. We might be able to apply this analysis to our system.

[8] A. E. Hosoi and John W. M. Bush. Evaporative instabilities in climbing films. *J. Fluid Mech.*, 442:217–239, 2001. This is Professor Hosoi's paper which was the starting point for this research. In it she derives the equation I'm working with and a lot of analytic results.

[9] A. Oron, S. H. Davis, and S. G. Bankoff. Long-scale evolution of thin liquid films. *Rev. Mod. Phys.*, 69(3):931–980, July 1997. A good background article describing thin-film, long-wavelength systems. One section is devoted to evaporatively driven systems like ours.

[10] Gilbert Strang. *Introduction to applied mathematics*. Wellesley-Cambridge Press, Wellesley, MA, 1986. Describes the discrete Fourier transform used in the pseudospectral method.

[11] L. Zhornitskaya and A. L. Bertozzi. Positivity-preserving numerical schemes for lubrication-type equations. *SIAM J. Numer. Anal.*, 37(2):523–555 (electronic), 2000. Suggests an alternative method for calculating our h terms in order to preserve positivity of our solution. Was used in the centered finite difference scheme to calculate h^3 term.